DOX-Loaded Gelatin Composite Hydrogels with Oxidation-Triggered Drug Release Property

[1]Chutong Shi, [1]Li Zhang, [2]Honglei Yin and [1]Haibin Gu*

[1]*Key Laboratory of Leather Chemistry and Engineering of Ministry of Education, Sichuan University, Chengdu 610065, China.*

[2]*Rongcheng Customs of Fuzhou Customs District of P. R. China, Fuzhou 350015, China.*

guhaibinkong@126.com*

(Received on 4th March 2020, accepted in revised form 23rd October 2020)

Summary: Hydrogels developed as stimuli-responsive drug delivery systems (DDSs) are increasingly concerned research focus in many fields such as chemistry, functional materials and biomedicine. Herein, we report the fabrication, characterization and drug release property of new gelatin composite hydrogels by using biocompatible gelatin and the doxorubicin (DOX)-loaded micelles of a redox-responsive side-chain ferrocene (Fc)-containing amphiphilic diblock copolymer PNFc-*b*-PNTEG (Fig. 1). The self-assembly method was firstly adopted to prepare the DOX-loaded micelles of PNFc-*b*-PNTEG with oxidation-sensitive release property, and the DOX-loaded gelatin composite hydrogels were then successfully fabricated by using blending and soaking methods, respectively. The formed hydrogels were characterized by many techniques including scanning electron microscope, energy-dispersive spectroscopy, differential scanning calorimetry, thermogravimetry and swelling test. The successful encapsulation of the DOX-containing micelles in the gelatin matrix was demonstrated, and the prepared composite hydrogels exhibited improved thermal stability, faster swelling speed and higher swelling ratios. The oxidation-triggered controlled *in vitro* release of DOX from the composite hydrogels was confirmed by using $FeCl_3$ at different concentrations as an oxidizing agent. The composite hydrogels could act as excellent solid carriers to guarantee the sustained-release effect of DOX, and it is feasible to keep the DOX molecules with high concentration at the specific site for a long period (20 days or so). Thus, the present composite hydrogels are anticipated to be good candidates as redox-responsive DDSs.

Keywords: Gelatin; Composite hydrogels; Doxorubicin; Redox-responsive; Ferrocene-containing polymer; Micelles; Drug delivery systems.

Introduction

Polymer-based drug delivery systems (DDSs), such as micelles, vesicles, polymer-drug conjugates, hydrogels and films, have attracted considerable interests of scientists in many fields including chemistry, functional materials and biomedicine [1-3]. Among them, hydrogels are three-dimensional polymer networks that are cross-linked by physical or chemical linkages and possess the ability to absorb and keep a large amount of water [4]. The insoluble bulk hydrogels are considered as excellent matrices of various drugs owing to their complimentary property of immobility once they are embedded or transfused into the specific site of treatment [5]. Moreover, hydrogels feature remarkable porosity and compatibility with aqueous environments [6], which afford them significant superiorities as drug delivery vehicles such as successive discharging of the encapsulated drug molecules [4,5]. And drug ingredients could be maintained with high local concentration at the treated sites for an extended period *via* various releasing mechanisms including diffusing, swelling and external stimuli [7].

Stimuli-responsive hydrogels, as one important subclass of hydrogels, are especially promising smart DDSs that can encapsulate drugs and controllably discharge them at the desirable sites under some specific triggers [8-10]. Especially, redox-responsive hydrogels are eye-catching because redox reactions are frequently found in various biological processes such as cellular respiration and apoptosis [11], and the dramatic difference in redox circumstances is also observed in the internal and external of cells as well as in normal and tumor tissue [12], thus many kinds of redox-sensitive linkages were adopted for this purpose [13].

Ferrocene (Fc)-containing polymers were also applied to fabricate various DDSs with redox-responsiveness, which is attributed to the reversible redox activity and stability of Fc unit under chemical or electrochemical action [14-16]. Most of the reported DDSs with redox-sensitive Fc moieties are

*To whom all correspondence should be addressed.

micelles [17], vesicles [18], nanocapsules [19], nanoparticles [20], nanotubes [21] and multilayer films [22]. However, the construction of DDSs *via* Fc-containing polymeric hydrogels is still a challenge, and there are few related reports [23,24]. Herein, we report the preparation of novel hydrogel DDSs by using biocompatible gelatin and a redox-responsive side-chain Fc-containing amphiphilic diblock copolymer (PNFc-*b*-PNTEG, Fig. 1). The doxorubicin (DOX)-loaded micelles with redox-responsiveness were firstly fabricated by the self-assembly of PNFc-*b*-PNTEG in the aqueous solution containing DOX, and the DOX-loaded gelatin hydrogels were then successfully prepared by blending and soaking methods, respectively. In the blending method, the DOX-loaded micellar solution of PNFc-*b*-PNTEG and gelatin were mixed at 50 °C, and then cooled to room temperature to get the gelatin composite hydrogel encapsulating DOX molecules. In the soaking method, the prefabricated pure gelatin hydrogel was immersed into the DOX-loaded micellar solution of PNFc-*b*-PNTEG to form the corresponding DOX-loaded hydrogel. The formed hydrogels were characterized by various techniques including scanning electron microscope (SEM), differential scanning calorimetry (DSC) and thermogravimetry (TG). The oxidation-triggered controlled *in vitro* release of DOX from the formed hydrogels was confirmed by using $FeCl_3$ as an oxidizing agent at different concentrations. The present drug-load hydrogels are anticipated to be good candidates as redox-responsive DDSs.

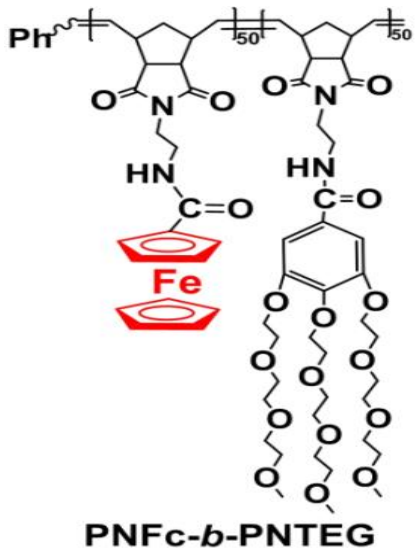

Fig. 1: Molecular structure of PNFc-*b*-PNTEG.

Experimental

Materials

The used amphiphilic diblock copolymer, PNFc-*b*-PNTEG, was synthesized following our previous method [25]. Gelatin (Type B, porcine skin), doxorubicin (DOX) and $FeCl_3$ were purchased from Energy Chemical, and used directly. All other chemicals were from commercial sources and used as received. All the solvents used were dried and freshly distilled.

Instrument

UV–vis absorption spectra were recorded using a Perkin-Elmer Lambda 19 UV-visible spectrometer. Scanning electron microscopy (SEM) images were recorded using a SM-7500F field emission SEM instrument (JEOL, Japan). An EDAX device, which is an accessory equipment of SEM, was applied to determine the energy-dispersive spectrum (EDS). The used voltage was 15 kv, and the aperture was 60 μm. Fluorescence spectra were measured using a fluorescence spectrophotometer (RF-5310PC, SHIMADZU, Japan). Dynamic light scattering (DLS) curves were determined using Malvern Zetasizer Nano-ZS series equipment (Malvern Instruments, UK) at 25 °C at an angle of 90°. Differential scanning calorimetry (DSC) measurements were performed using DSC1/700 (Mettler Toledo, Switzerland) and the sample was heated from 0 °C to 200 °C at 10 °C/min under N_2 atmosphere. Thermogravimetry/derivative thermogravimetry (TG/DTG) analysis was conducted using TGA/DSC2/1600 (Mettler Toledo, Switzerland) from 30 °C to 800 °C at a heating rate of 10 °C/min under N_2 atmosphere.

Fabrication of DOX-loaded micelles of PNFc-b-PNTEG

1 mL of DMF (*N*,*N*-dimethylformamide) in a vial was firstly adopted to dissolve completely the PNFc-*b*-PNTEG (2.5 mg) and DOX (5.0 mg). 9 mL of deionized water was then injected drop-by-drop into the vial under dramatically stirring condition. The formed mixture was further agitated vigorously at room temperature (RT, 25 °C) for 2h. After that, the mixture was transferred into a dialysis bag with MWCO (molecular weight cut off) of 3500 Da, and the dialysis treatment was conducted against deionized water at RT for 3 days to get rid of the DMF

solvent and the unencapsulated DOX. The loaded DOX in the formed micelles of PNFc-*b*-PNTEG could be determined by using UV–vis spectrophotometry. The absorbance at 485 nm, which is the maximum absorption (λ_{max}) of DOX, was recorded, and the loaded DOX could be calculated using the standard curve of DOX (Fig. 2). The following two formulas were adopted to calculate the two parameters of loading effect, namely, loading content (LC) and encapsulation efficiency (EE) [25].

$$LC(\%) = \frac{W_{loaded\ DOX}}{W_{micelles}} \times 100\%$$

$$EE(\%) = \frac{W_{loaded\ DOX}}{W_{added\ DOX}} \times 100\%$$

Thereinto, $W_{\text{loaded DOX}}$ is the amount of DOX (mg) encapsulated by the micelles of PNFc-*b*-PNTEG and W_{micelles} is the amount of micelles of PNFc-*b*-PNTEG used (mg), while W_{added} DOX is the amount of DOX added during the loading process.

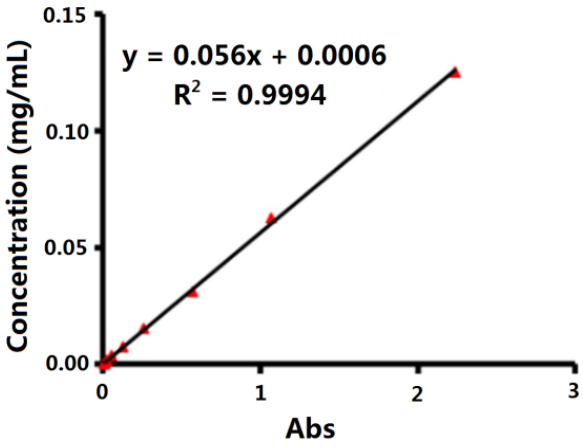

Fig. 2: The standard curve of DOX in water by using its UV–vis absorption at 485 nm.

Oxidation-triggered DOX release from micelles of PNFc-b-PNTEG

$FeCl_3$ was used as the oxidizing agent to carry out the DOX release experiments, and its concentrations were 0, 400, and 600 μmol L^{-1}, respectively. Concretely, 5 mL of the prepared DOX-loaded micelles of PNFc-*b*-PNTEG was injected into a dialysis bag with MWCO of 3500 Da, and the dialysis treatment was then conducted at RT against the $FeCl_3$ aqueous solution (30 mL). At different intervals, the released DOX was determined using the UV–vis spectroscopy. The obtained absorbance value at 485 nm was used to calculate the amount of released DOX using the standard curve of DOX. The release profile was drawn using the calculated values as the Y-axis and the treatment time as X-coordinate.

Fabrication of gelatin composite hydrogels containing DOX-loaded micelles of PNFc-b-PNTEG

In the blending method, the prepared DOX-loading micellar solution of PNFc-*b*-PNTEG was used as the solvent to dissolve gelatin. Concretely, 1.0 g of gelatin was added in a vial, and 5 mL of the DOX-loading micellar solution of PNFc-*b*-PNTEG was then added into the vial. The obtained mixture was dramatically agitated at 50 °C for 10 min to get the transparent solution. The gelatin composite hydrogel was then obtained by cooling the solution to RT, and labeled as DOX-gel-1.

The soaking method was also used to prepare the gelatin composite hydrogel containing DOX-loading micelles of PNFc-*b*-PNTEG. The pure gelatin hydrogel was firstly fabricated by cooling the gelatin (1.0 g) aqueous solution (5 mL) from 50 °C to RT. The formed hydrogel was then lyophilized. The gelatin composite hydrogel was fabricated by soaking the dried hydrogel into 30 mL of the prepared DOX-loading micellar solution of PNFc-*b*-PNTEG. The soaking treatment was conducted at RT for 2 days, and the resulting product was called as DOX-gel-2.

Oxidation-triggered DOX release from gelatin composite hydrogels

The dialysis method was adopted to conduct the release experiments using the $FeCl_3$ aqueous solution with the concentrations of 0, 400, and 600 μmol L^{-1}, respectively. Specifically, 1.0 g of the lyophilized gelatin composite hydrogel (DOX-gel-1 or DOX-gel-2) was put in a dialysis tube (MWCO=3500), and the dialysis operation was then carried out at RT against the $FeCl_3$ aqueous solution (30 mL). During this period, the released DOX was measured *via* the UV–vis spectroscopy. The obtained absorbance value at 485 nm was applied to calculate the amount of released DOX using the standard curve of DOX (Fig. 2). The release curve was drawn using the calculated values as the vertical coordinate and the treatment time as the horizontal axis.

Measurement of swelling ratio of hydrogels

The tested hydrogel was firstly freeze-dried and weighed as W_1 (mg). Then, the dried hydrogel were immersed at RT into the deionized water (200 mL). During this period, the sample was taken out at some time point, and the water on its surface was absorbed quickly using filter paper, and it was weighed as W_t (mg). The following formula was then used to calculate its swelling ratio (SR).

$$SR = \frac{w_t - w_1}{w_1} \times 100\%$$

Results and Discussion

*Fabrication of DOX-Loaded micelles of **PNFc-b-PNTEG***

Amphiphilic Fc-containing polymers could be developed to be smart drug carriers owing to the revisable redox property of Fc units [26-28]. In this study, the used amphiphilic block copolymer PNFc-*b*-PNTEG (Fig. 1) contains the hydrophobic Fc-containing block and hydrophilic block bearing the dendronized triethylene glycol (TEG) groups. Using the known two-step sequential ring-opening metathesis polymerization (ROMP) method [25], this well-defined polymer was successfully synthesized with 50 of polymerization degrees for both two blocks by controlling the feed molar ratio of its two monomers to the Grubbs' 3rd generation catalyst. The obtained **PNFc-*b*-PNTEG** was fully characterized by ^{1}H NMR, ^{13}C NMR, IR and UV-vis spectra, and its molecular weight was determined by gel permeation chromatography (GPC) and the ^{1}H NMR end-group analysis. All these results were listed in the supplementary information (SI).

Amphiphilic polymers could self-assemble into various nanostructures only when the used concentrations are beyond their critical micelle concentrations (CMCs) [29]. Herein, the CMC value of PNFc-*b*-PNTEG was thus measured following the typical pyrene fluorescence probe method [30]. Fig. 3a shows the recorded fluorescence spectra of the mixture of pyrene and PNFc-*b*-PNTEG at different concentrations. According to Fig. 3a, a series of ratios between the intensities at 383 nm (I_3) and those at 372 nm (I_1) were calculated at the corresponding concentrations of PNFc-*b*-PNTEG. The profile shown in Fig. 3b was then drawn using the obtained ratios and the corresponding logarithmic concentrations of PNFc-*b*-PNTEG as the vertical and horizontal coordinates, respectively. The CMC value of PNFc-*b*-PNTEG was determined to be 0.1 mg mL^{-1} following the reported tangent method [30]. Based on this result, a concentration of 1.0 mg mL^{-1}, which is much larger than the measured CMC, was adopted in the following experiments to prepare the micelles of PNFc-*b*-PNTEG and the corresponding DOX-containing micelles using the self-assembly method [30].

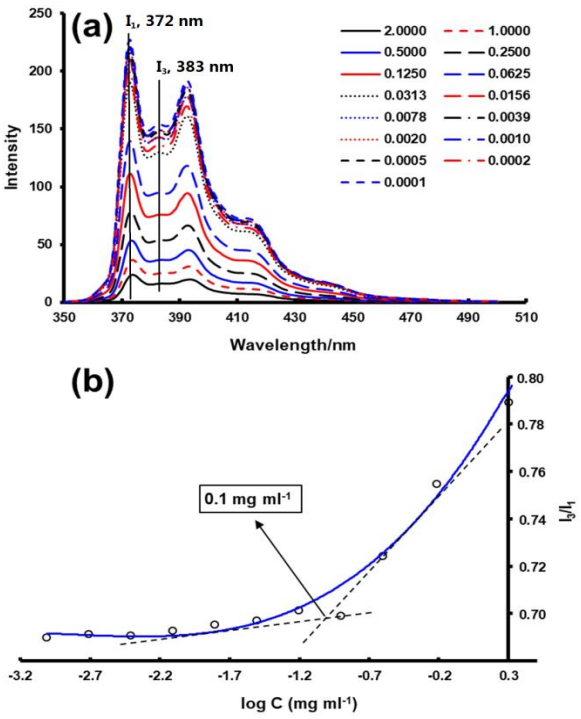

Fig. 3: CMC determination of PNFc-*b*-PNTEG. (a) Fluorescence spectra of the mixture of PNFc-*b*-PNTEG (from 0.0001 to 0.2 mg mL^{-1}) and pyrene in water. (b) Profile of I_3/I_1 *versus* the logarithmic concentration of PNFc-*b*-PNTEG aggregate solution.

Both empty micelles and the ones encapsulating anticancer drug of DOX were prepared by the typical dialysis procedure [31], and the morphology and size of the formed micelles were analyzed by SEM and DLS, respectively. As shown in Fig. 4, the torispherical shape was observed for the empty and DOX-containing micelles of PNFc-*b*-PNTEG. The formation of micelles was driven by the amphiphilicity of PNFc-*b*-PNTEG. During the self-assembly of PNFc-*b*-PNTEG macromolecules in water, as expected, the

hydrophobic Fc-containing blocks aggregated into the cores of micelles to keep away from the water medium, while the hydrophilic TEG-containing blocks covered over the cores as the peripheries of micelles owing to its high affinity to water solvent. During this period, the hydrophobic DOX molecules were also encapsulated into the micellar cores, which is attributed to the theory that similarities can be solvable easily in each other [28-31]. Thus, the formed micelles could exist stably in water as the combined result of these actions.

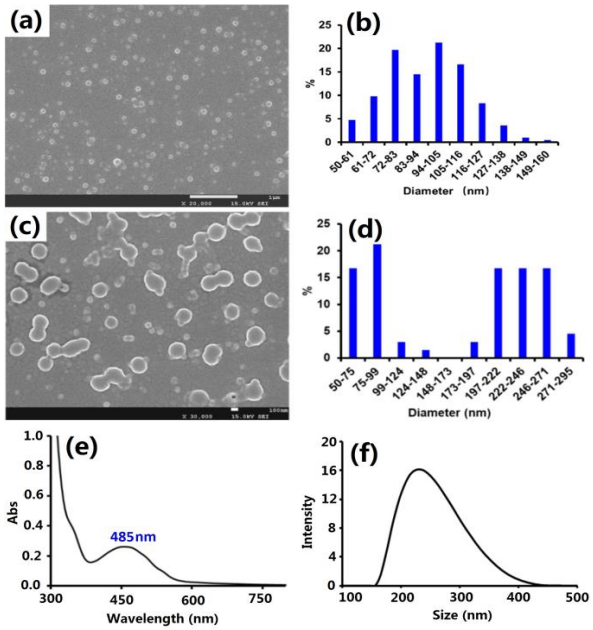

Fig. 4: SEM image (a) and size distribution (b) of micelles of PNFc-*b*-PNTEG. SEM image (c) and size distribution (d) of DOX-loading micelles of PNFc-*b*-PNTEG. UV-vis spectrum (e) and DLS curve (f) of DOX-loading micelles of PNFc-*b*-PNTEG.

For the empty micelles, the particle size of 90 ± 20 nm is provided by SEM (Fig.4b), while the DLS analysis (not shown) indicated an average hydrodynamic diameter of 123 nm with PDI (polydispersion index) of 0.121. The size difference provided by SEM and DLS could be explained by their different determination conditions [25,28,30]. Interestingly, the SEM image (Fig. 4c) illustrates two different size distributions for the formed DOX-loaded micelles. As shown in Fig.4d, one is 89 ± 40 nm, which is very close to the size of empty micelles. This comparison confirms that a part of micelles have no DOX molecules encapsulated during the fabrication process of drug-loaded micelles of PNFc-*b*-PNTEG. Another size distribution is found to be 235 ± 50 nm, which is much larger than the size of empty micelles. This increase in size could be attributed to the successful encapsulation of DOX molecules by these micelles of PNFc-*b*-PNTEG [25,29,30]. The loading of DOX was also proved by the UV-vis spectrum of the resulting micelles (Fig.4e). In this curve, a maximum absorption peak is observed at 485 nm, and this peak could be regarded as the characteristic λ_{max} of DOX. The encapsulated-DOX was then quantitatively measured using the standard profile of DOX (Fig. 2). The obtained LC and EE values were calculated to be 4.7% and 9.4%, respectively, when the concentration of PNFc-*b*-PNTEG reached 1.0 mg mL^{-1}. In addition, the particle size of DOX-loaded micelles was also characterized by DLS method. The average hydrodynamic diameter is found to be 302 nm with PDI of 0.291. The DLS result also indicates the bigger size of the drug-loaded micelles of PNFc-*b*-PNTEG. Notably, the bigger PDI value, indicating the wider size distribution of particles, is also obtained, which is attributed to the coexistence of empty and DOX-containing micelles in the final product.

Oxidation-triggered release of DOX from micelles of ***PNFc-b-PNTEG***

The chemical or electrochemical treatments could lead to the conversion of neutral Fc group into cationic ferricinium (Fc^+) units [16]. When this transformation takes place, Fc-containing polymers with electric neutrality could change into Fc^+-containing polyelectrolytes with electric positivity. Accordingly, the charge balance can be broken in the interior of a micelle and between different micelles. The original micelles could disappear or convert into swelling ones, which depends on the types and intensity of external redox stimuli [16]. Thus, the loaded-drug molecules could be released *in vitro* or *in vivo* with the action of specific redox stimuli. Herein, we used the $FeCl_3$ aqueous solutions with different concentrations (0, 400 and 600 μmmol L^{-1}) as the oxidizing agents to investigate the *in vitro* release behavior of DOX from micelles of PNFc-*b*-PNTEG. Fig. 5 provides the resulting three release profiles. When these curves are compared, it can be concluded that the higher the concentration of $FeCl_3$, the faster the release rate of DOX. Specifically, when there is no oxidizing agent, namely the concentration of $FeCl_3$ is 0 μmmol L^{-1}, the release amount of DOX is almost negligible. In the first 9 h, the release percent of encapsulated DOX reached only 6.6%, and after 93 h of dialysis treatment, the value of 11.5% was obtained. In the early period,

the released DOX probably is belong to the unloaded ones, and in the subsequent stage, the slight release of DOX should be driven by the diffusion action that is resulted from the concentration difference of DOX between the inside and outside of dialysis bag [29,30]. However, the low release amount obtained indicates that the diffusion action is not strong enough to promote the rapid release of loaded DOX in the micelles of PNFc-*b*-PNTEG. Unlike the case of the control group, both experimental groups with 400 and 600 μmmol L^{-1} of $FeCl_3$, respectively, witnessed the explosive release of DOX, especially in the early period. To be specific, during the first 9 h, the release ratios were increased to 23.9% and 29.0%, respectively. The rapid and almost exponential release of DOX could be found in the first 45 h or so. Concretely, at 400 μmmol L^{-1} of $FeCl_3$, the determined releasing percent was 56.1%, and when the concentration of $FeCl_3$ was improved to 600 μmmol L^{-1}, the corresponding releasing rate was increased to 63.6%. However, after this period, the release rate of DOX sharply slowed down. It can be seen that the final release ratios are 60.0% and 70.2%, respectively, after 93 h of dialysis treatment with 400 and 600 μmmol L^{-1} of $FeCl_3$. There is no dramatic improvement for the release amount of DOX during the second half period of dialysis treatment. This could be attributed to the more and more severe aggregation of oxidized PNFc-*b*-PNTEG formed by the disassembly of its micelles. This process probably leaded to the encapsulation of unoxidized micelles into these large aggregates, thus it could be more and more difficult for these micelles to release the loaded DOX molecules [25, 29, 30].

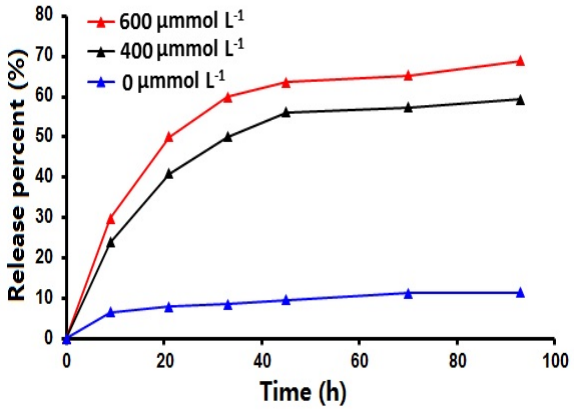

Fig. 5: Release curves of DOX from micelles of PNFc-*b*-PNTEG treated by $FeCl_3$ at different concentrations.

In order to further explore the release process, the DLS method was applied to detect the particle size change of the PNFc-*b*-PNTEG micelles containing DOX during the period of treatment with $FeCl_3$ aqueous solution. Fig.6a shows the DLS curves of the treated micelles during the first 3.5 h, while Fig.6b provides time-dependent average size change of these micelles. Notably, the treatment of $FeCl_3$ as an oxidizing agent of Fc units can lead to the change of the original DLS curve with one peak into the ones with two peaks. For example, after 0.5 h of dialysis treatment with $FeCl_3$, the resulting DLS profile possess one peak at 250 nm or so, whose location and shape is similar to that of original DLS curve (0 h), and a new peak at about 600 nm is observed. The appearance of the new peak with bigger size could be explained by following two points. One is that the core size of micelles is increased as a result of charge repulsion by Fc^+ units resulted from the oxidation by $FeCl_3$. Another reason is that aggregation of several micelles results in the formation of aggregates with bigger size. As expected, the intensity of peak at about 250 nm is gradually decreased with the prolonged treatment time, which indicates that the number of unoxidized micelles is fewer and fewer. Moreover, as the treatment time goes on, an obvious right shift is observed for the new peak and its width is dramatically improved. These results indicate that the newly formed aggregates have gradually increased particle size, and the corresponding range of size distribution is wider and wider. Accordingly, as shown in Fig.6b, while the treating time was prolonged, the average particle size of treated micelles exhibit a gradually increase trend. Specially, the mean size was improved from the original 300 nm or so to about 1200 nm after 3.5 h of treatment. In short, the time-dependent DLS analysis further demonstrates the oxidation-triggered drug release property of the **PNFc-*b*-PNTEG** micelles containing DOX.

Fabrication of DOX-Loaded gelatin composite hydrogels

Smart hydrogels, as desirable DDSs, possess several critical advantages such as providing suitable region for drug storage, controlling the releasing rate of drug under specific stimuli, modifying the undesirable properties (e.g. bitter taste, odor), etc [32-34]. Especially, the application of hydrogels as DDSs is beneficial for promoting the therapeutic efficacy of lipophilic drugs in the side of improving solubility, dispersibility, bioavailability and *in vivo* stability [34]. In this study, we further explored the effective methods to upload the hydrophobic

anticancer drug of DOX encapsulated in the micelles of PNFc-*b*-PNTEG to a gelatin hydrogel system, and the fabricated gelatin composite hydrogels were well investigated in terms of interior structure, thermostability, swelling property and the release behavior of DOX loaded.

Gelatin is one of the functional materials frequently used drug delivery owing to its appealing advantages such as good water solubility, good biodegradability, excellent biocompatibility, low antigenicity and low price [4]. Thus, gelation was here adopted as the main matrix to build composite hydrogels as DDSs. Using the above prepared DOX-containing micelles of PNFc-*b*-PNTEG as one starting material, the gelatin composite hydrogels were fabricated by blending and soaking methods, respectively. The DOX-containing gelatin composite hydrogels were successfully prepared using both methods, and their structure and properties were fully characterized and compared by various analysis techniques including SEM, EDS, DSC, TG, swelling test and DOX-releasing experiments.

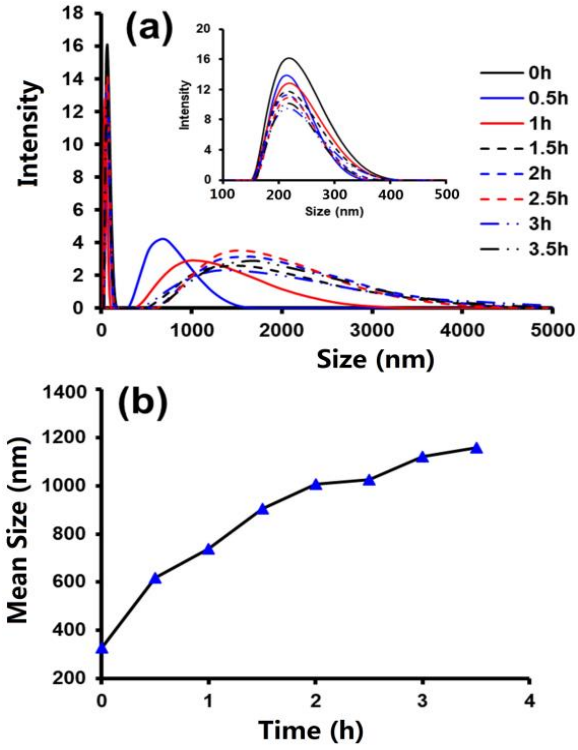

Fig. 6: DLS curves (a) and average particle sizes (b) of DOX-loading micelles of PNFc-*b*-PNTEG treated in $FeCl_3$ aqueous solution (600 μmol L^{-1}) at different time.

SEM analysis

Fig. 7. provides the SEM images of the DOX-Gel-1 fabricated by the blending method and DOX-Gel-2 prepared by the soaking method, and the microstructure of the corresponding pure gelatin hydrogel (Gel) was also observed by SEM for comparison purpose. As can be seen in Fig.7a, 7c and 7e, all the hydrogels exhibit typical honeycomb-like internal microstructure [14]. It is worth noting that the difference in pore size distribution was found in these hydrogels, which could be attributed to their different fabrication methods. To be specific, the pore size distributions were measured to be 85 ± 56 μm for Gel (Fig. 7b), 132 ± 74 μm for DOX-Gel-1 (Fig. 7d)and 210 ± 90 μm for DOX-Gel-2 (Fig. 7f), respectively. Obviously, the two gelatin composite hydrogels containing the micelles of PNFc-*b*-PNTEG have bigger pore size than the pure gelatin hydrogel, which is attributed to the introduction of the DOX-loaded micelles. As expected, the different fabrication methods can also result in different pore size distributions. The pore size of DOX-Gel-2 is bigger than that of DOX-Gel-1. The reason for this difference may be that the long-time immersion of gelatin hydrogel in the DOX-containing micellar solution of PNFc-*b*-PNTEG leads to its excessive expansion and the abundant water absorbed. Thus, when DOX-Gel-2 was further freeze-dried, the ice crystals with large volume could form in the interior of hydrogel matrix, and the remove of them could lead to the appearance of the big pores [14]. At the same time, EDS determination, which is accompanied by SEM, was conducted to qualitatively detect the element distribution in microscopic areas of hydrogels. As shown in Fig. 7g and 7h, besides C N and O elements that are often found in organic materials, there is iron (Fe) element in both hydrogels of DOX-Gel-1 and DOX-Gel-2. Fe is the characteristic element of Fc units in the molecular structure of PNFc-*b*-PNTEG. Thus, we have the reason to believe that the DOX-containing micelles could be encapsulated successfully into the inside of gelatin hydrogels by both blending and soaking methods used in this work. Namely, both two methods are feasible to fabricate DOX-loaded gelatin composite hydrogels.

DSC and TG analysis

According to the above analysis, we can confirm that there are DOX-loaded micelles of PNFc-*b*-PNTEG in the formed composite hydrogels of DOX-Gel-1 and DOX-Gel-2. The introduction of these micelles may change the thermal property of the resulting hydrogels. Therefore, the DSC and TG determinations were further carried out for the prepared

composite hydrogels, and the obtained results were compared with that of gelatin hydrogel without DOX-containing micelles.

Fig. 8 shows the DSC curves of Gel, DOX-Gel-1 and DOX-Gel-2. In each DSC curve, only one peak is observed during the range 0-150 °C. These peak temperatures are the glass transition temperature (T_g) of materials, and reflect the thermal denaturation temperature of hydrogels. The determined T_g values are 72.3 °C for Gel, 74.1 °C for DOX-Gel-1 and 75.3 °C for DOX-Gel-2, respectively. Noticeably, the introduction of the DOX-loaded micelles of PNFc-*b*-PNTEG slightly improves the thermal stability of gelatin hydrogels, which is probably attributed to the physical intertwinement [14, 15] between gelatin macromolecules and the polymeric chains of PNFc-*b*-PNTEG.

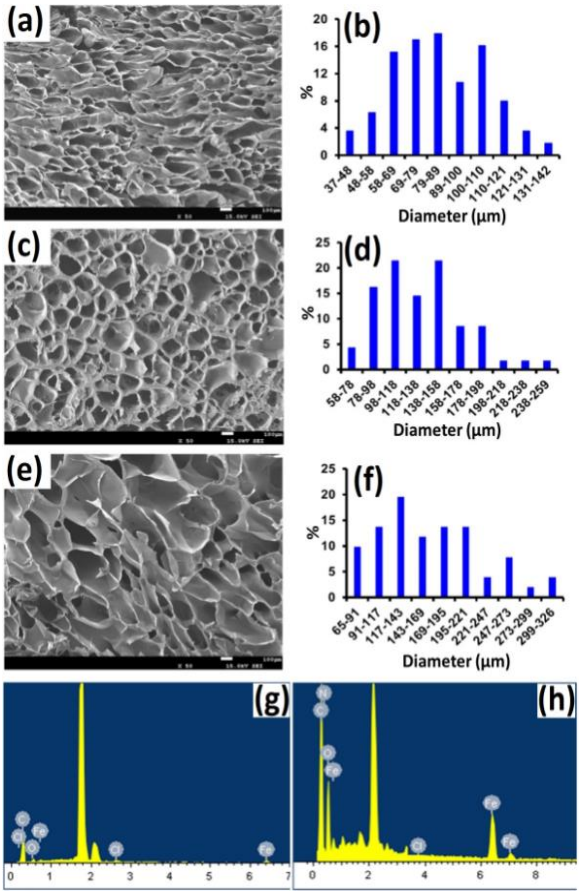

Fig. 7: SEM images and pore size distributions of Gel (a,b), DOX-Gel-1 (c,d) and DOX-Gel-2 (e,f). EDS results of DOX-Gel-1 (g) and DOX-Gel-2 (h).

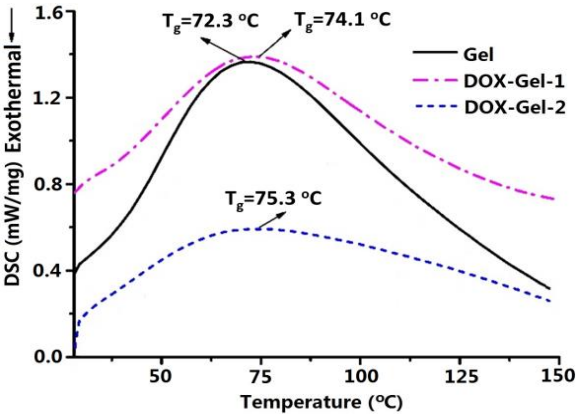

Fig. 8: DSC curves of Gel, DOX-Gel-1 and DOX-Gel-2.

TG is another important tool to characterize the thermal stability of materials. Because of the difference in structure and composition, different materials exhibit diverse characteristics in thermal decomposition temperature and weight loss rate. The blending of materials can also affect the thermal stability of the resulting products. Fig. 9 provides the measured TG and DTG curves of Gel, DOX-Gel-1 and DOX-Gel-2. As shown in Fig. 9a, all the TG curves exhibit the smooth reverse S shape, and the thermal decomposition process can be divided into three stages in the range of 30-700 °C. To be specific, the weight loss between 30 °C and 120 °C could be regarded as the first stage that is assigned to the evaporation loss of residual water in the hydrogels. As shown in Table-1, the corresponding weight loss ratios are 9.28% for Gel, 10.46% for DOX-Gel-1 and 2.77% for DOX-Gel-2, respectively. Gel and DOX-Gel-1 exhibit higher weight loss rates in this stage, which may be due to the fact the water included in the hydrogels is not fully removed during the freeze drying process. To eliminate the effect of residual water, as shown in Table-1, the following weight loss ratios and residual rates were further calculated when the water content is totally removed. The weight loss in the range of 120-500 °C could be deemed as the second stage of thermal decomposition. This stage is corresponding to the decomposition of main components of gelatin [14, 15]. The corrected values based on absolute dry hydrogels are 74.33% for Gel, 70.45% for DOX-Gel-1 and 67.15% for DOX-Gel-2, respectively. Notably, both DOX-Gel-1 and DOX-Gel-2 have lower weight loss ratios than Gel in this stage, indicating their thermal stability could be improved by the introduction of the DOX-loaded micelles of PNFc-*b*-PNTEG. This results are in keeping with ones of the above DSC measurements. Furthermore, this viewpoint was also proved by the calculated values of the maximum thermal decomposition temperatures

(T_{max}) for the three hydrogels. As shown in Fig. 9b, Gel has a T_{max} of 313.7 °C, while the T_{max} values were increased to 320.3 °C (DOX-Gel-1) and 318.4 °C (DOX-Gel-2), respectively. These results indicate that when the DOX-loaded micelles were introduced by the blending or soaking methods, their interaction with gelatin molecules is beneficial for improving the thermal stability of hydrogel framework. The range of 500-700 °C is the third weight loss stage of the TG curves, and this stage is reuslted from the further thermal degradation of gelatin ingredients and other orgianic components included [14,15]. All the hydrogels exhibit low weight loss ratio in the third stage, and the obtained values are 3.43% for Gel, 2.08% for DOX-Gel-1 and 2.69% for DOX-Gel-2, respectively. It is worth reminding that distinctly different residual rates were observed between the pure gelatin hydroge and composite ones. Gel possesses the lowest residual rate of 22.24%, indicating its worst thermal stability. As expected, the formed gelatin composite hydrogels exhibit the increased residual rates, and the values are 27.47% for DOX-Gel-1 and 30.16% for DOX-Gel-2, respectively. The increased residues should be resulted from the decomposition products of PNFc-*b*-PNTEG, especially the organic oxide of iron [15]. These results further demonstrate the improvement of composite hydrogel in thermal stability.

Swelling ratio (SR) is a very important index to indicate the water absorbing capacity of hydrogel, and is also crucial for the application of hydrogels as DDSs [32,33]. Thus, the swelling kinetics of the hydrogels prepared in this study was determined, and the corresponding swelling curves are listed in Fig. 10. It is very clear that the DOX-loaded gelatin composite hydrogels exhibit the faster swelling rate and higher SR than the pure gelatin hydrogel. For example, in the first 0.5 h of soaking, the determined SRs are 124.5% for Gel, 757.2% for DOX-Gel-1 and 176.2% for DOX-Gel-2, respectively. And after 32h, the final SR of Gel is only 1115.2%, while the corresponding SRs reach 1323.1% for DOX-Gel-1 and 1193.1% for DOX-Gel-2, respectively. Notably, although Gel and DOX-Gel-2 have different values of SRs at the same soaking time, their swelling curves possess similar shape, namely they have similar swelling kinetics. Concretely, they exhibit relatively slow swelling rate, and 24 h are needed for them to achieve the equilibrium swelling state. On the contrary, DOX-Gel-1 possesses rapid swelling rate, especially in the first 3 h of soaking treatment, and it took only 5 h or so to reach almost the balance of swelling. Obviously, the introduction of DOX-loaded micelles of PNFc-*b*-PNTEG is helpful to increase the water absorbing capacity of the resulting gelatin composite hydrogels, which is probably attributed to the larger pore size of these hydrogels and the hydrophilic periphery of micelles [30]. On the other hand, the fabrication method of hydrogels could also affect their water absorbing behaviors. DOX-Gel-2 prepared by the soaking method exhibits much slower swelling speed than DOX-Gel-1 fabricated by the blending method, although the former has slight bigger pore size than the latter. This is could be explained by the more evenly distribution of pore size of DOX-Gel-1 prepared by blending method, which is more conducive to the flow of water molecules [4].

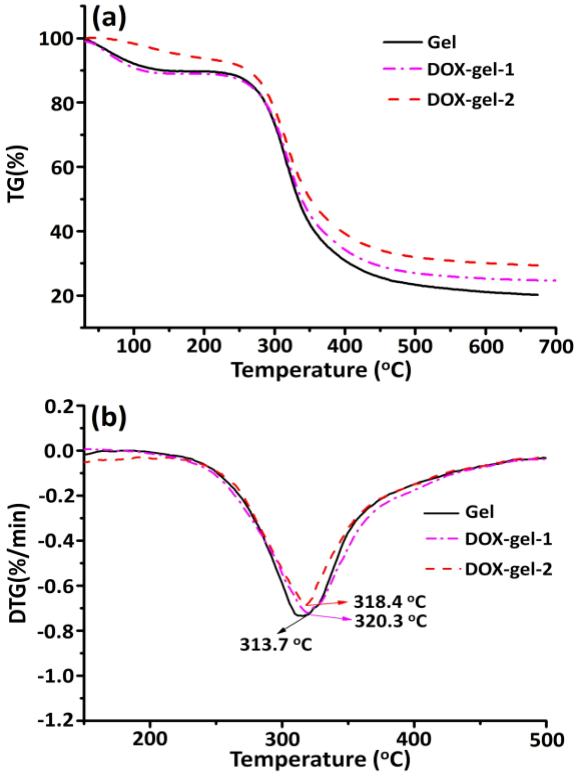

Fig. 9: TG (a) and DTG (b) curves of Gel, DOX-Gel-1 and DOX-Gel-2.

Table-1: Weight loss ratio (%) of hydrogels from TG curves.

Hydrogel	The first stage (30-120 °C)	The second stage (120-500 °C)	The third stage (500-700 °C)	Residual rate
Gel	9.28	67.43/74.33[a]	3.11/3.43[a]	20.18/22.24[a]
DOX-Gel-1	10.46	63.08/70.45[a]	1.86/2.08[a]	24.60/27.47[a]
DOX-Gel-2	2.77	65.29/67.15[a]	2.62/2.69[a]	29.32/30.16[a]

[a] Values calculated when the water content is totally removed, namely, the weight loss ratio or residual rate of hydrogel without water.

Swelling property of hydrogels

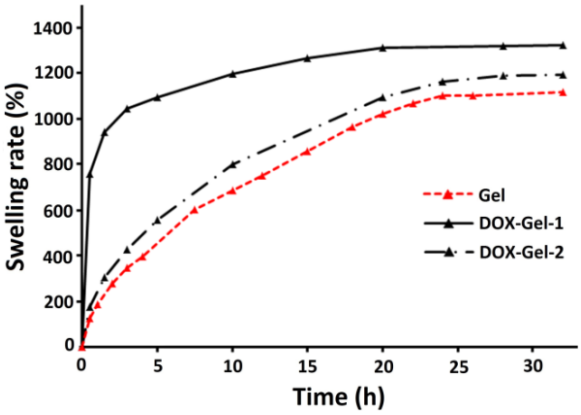

Fig. 10: Swelling curves of Gel, DOX-Gel-1 and DOX-Gel-2.

Oxidation-triggered release of DOX from gelatin composite hydrogels

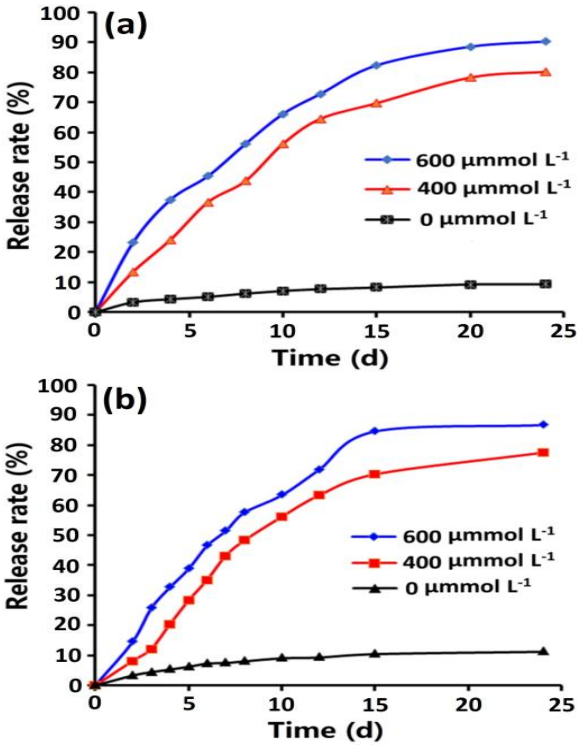

Fig. 11: DOX release profiles of DOX-Gel-1 (a) and DOX-Gel-2 (b) at different concentrations of $FeCl_3$.

The *in vitro* releasing kinetics of DOX encapsulated in the gelatin composite hydrogels, DOX-Gel-1 and DOX-Gel-2, was investigated by using $FeCl_3$ as the oxidizing agent. The typical dialysis procedure [29,30] was adopted in these experiments, and the UV-vis spectroscopy was used to detect the releasing DOX in the dialysate. Fig. 11 shows the obtained releasing curves under different concentrations of $FeCl_3$. It is obvious that $FeCl_3$ can trigger the release of DOX in both composite hydrogels, and the higher its concentration, the faster the release rate of DOX. When there is no $FeCl_3$, the release percent of DOX is almost negligible (less than 10%) after the long period (24 days) of dialysis treatment. On the contrary, a lot of DOX could be released in the presence of $FeCl_3$. Concretely, when the concentration of $FeCl_3$ is 400 μmol L^{-1}, the final release rates are 79.2% for DOX-Gel-1 and 75.4% for DOX-Gel-2, respectively. And when the concentration is improved to 600 μmol L^{-1}, the release rates at 24 days are measured to be 90.4% for DOX-Gel-1 and 87.8% for DOX-Gel-2, respectively. Notably, the similar release kinetics of DOX is observed under different concentrations of $FeCl_3$. For DOX-Gel-1, it took 20 days to reach the equilibrium release period; while for DOX-Gel-2, 15 days are needed to achieve this stage. In other words, the release rate of DOX from DOX-Gel-1 is slower than that from DOX-Gel-2, which could be explained by the different loading methods of DOX. The blending method probably leads to the deeper and evener encapsulation of DOX-containing micelles in the gelatin hydrogel matrix, and the resulting DOX-Gel-1 exhibit the denser microstructure. On the contrary, in the soaking method, the DOX-containing micelles are mainly located in outer space of hydrogel network owing to the steric hindrance, and the loose microstructure of DOX-Gel-1 is beneficial for the more rapid release of DOX encapsulated. However, the release speed of DOX from these composite hydrogels is dramatically slower that that from the micellar solution of PNFc-*b*-PNTEG. This release property could lead to the sustained-release effect of drug, and thus the high concentration of drug could be kept in the specific site for a long time.

Conclusion

In this study, we successfully fabricated the DOX-containing micelles with oxidation-triggered release property by using a polynorbornene-based amphiphilic diblock copolymer PNFc-*b*-PNTEG containing redox-sensitive hydrophobic ferrocene units and hydrophilic dendronized triethylene glycol groups in the side chain. And these micelles were then used to prepare DOX-encapsulated gelatin composite

hydrogels by the blending and soaking methods, respectively. The obtained hydrogels were fully investigated in terms of microstructure, thermal stability, swelling property and the *in vitro* DOX-release behavior, and the following conclusions could be reached.

1 Both blending and soaking methods are feasible in the preparation of DOX-containing gelatin composite hydrogels by using the DOX-loaded micelles of PNFc-*b*-PNTEG and gelatin as the starting materials. The encapsulation of these micelles cannot alter the honeycomb-like microstructure of gelatin hydrogel, but the formed composite hydrogels exhibit increased pore size, especially the one fabricated by soaking method.

2 Compared with the pure gelatin hydrogel, the DOX-containing gelatin composite hydrogels possess not only the improved thermal stability, but also the faster swelling speed and higher swelling ratios.

3 The DOX encapsulated in the gelatin composite hydrogels could be controlled released in the presence of $FeCl_3$ as the oxidizing agent of ferrocene groups. The higher the concentration of $FeCl_3$, the faster the release speed of DOX. The present hydrogels could act as excellent solid carriers to guarantee the sustained-release effect of DOX, and it is feasible to keep the drug molecules with high concentration at the specific site for a long period (20 days or so). Thus, the gelatin composite hydrogels fabricated by the blending and soaking methods in this work have great potential to be used as effective drug delivery systems for the application in the biomedical field.

Supplementary material

The synthesis and characterization data of the diblock copolymer PNFc-*b*-PNTEG, including ^{1}H NMR, ^{13}C NMR, IR, UV-vis, GPC and end-group analysis, were listed in the supplementary material. These data can be obtained free of charge at the website of this journal or by contacting the corresponding author of Dr. H. Gu *via* the email of guhaibinkong@126.com.

Acknowledgements

This work was financially supported by the National Natural Science Foundation of China (No. 21978180) and the Science & Technology Department of Sichuan Province (No. 2018HH0038). The author of Chutong Shi was funded by the Innovation Training Program for college students of Sichuan University (C2019104671). The authors thank Jinwei Zhang (College of Biomass Science and Engineering, Sichuan University) for his help in the SEM analysis.

References

1. X. Guo, L, Wang, X. Wei and S .B. Zhou, Polymer-Based Drug Delivery Systems for Cancer Treatment, *J. Polym. Sci. Pol. Chem.*, **54**, 3525 (2016).
2. H. H. Xiao, L. S. Yan, E. M. Dempsey, W. T. Song, R. G. Qi, W. L. Li, Y. B. Huang, X. B. Jing, D. F. Zhou, J. X. Ding and X. S. Chen, Recent progress in polymer-based platinum drug delivery systems, *Prog. Polym. Sci.*, **87**, 70 (2018).
3. S. D. Mu, W. T. Liu, Q. J. Ling, X. Liu and H. B. Gu, Ferrocenyl Amphiphilic Janus Dendrimers as Redox-Responsive Micellar Carriers, *Appl. Organomet. Chem.*, **33**, e4908 (2019).
4. Q. X. Zhao, S. D. Mu, Y. R, Long, J. Zhou, W. Y. Chen, D. Astruc, C. Gaidau and H. B. Gu, Tannin-Tethered Gelatin Hydrogels with Considerable Self-Healing and Adhesive Performances, *Macromol. Mater. Eng.*, **304**, 1800664 (2019).
5. A. Onaciu, R. A. Munteanu, A. I. Moldovan, C. S. Moldovan and I. Berindan-Neagoe, Hydrogels Based Drug Delivery Synthesis, Characterization and Administration, *Pharmaceutics*, **11**, 432 (2019).
6. Q. X. Zhao, S. D. Mu, X. Liu, G. R. Qiu, D. Astruc and H. B. Gu, Gallol-Tethered Injectable AuNP Hydrogel with Desirable Self-Healing and Catalytic Properties, *Macromol. Chem. Phys.*, **220**, 1800427 (2019).
7. M. Ejaz, H. N. Yu, Y. Yan, D. A. Blake, R. S. Ayyala and S. M. Grayson, Evaluation of redox-responsive disulfide cross-linked poly(hydroxyethyl methacrylate) hydrogels, *Polymer*, **52**, 5262 (2011).
8. K. S. Soppimath, T. M. Aminabhavi, A. M. Dave, S. G. Kumbar and W. E. Rudzinski, Stimulus-responsive "smart" hydrogels as novel drug delivery systems, *Drug Dev. Ind. Pharm.*, **28**, 957 (2002).
9. M. C. Koetting, J. T. Peters, S. D. Steichen and N. A. Peppas, Stimulus-responsive hydrogels: Theory, modern advances, and applications, *Mater. Sci. Eng. R-Rep.*, **93**, 1 (2015).
10. N. Sood, A. Bhardwaj, S. Mehta and A. Mehta, Stimuli-responsive hydrogels in drug delivery

and tissue engineering, *Drug Deliv.*, **23**, 758 (2016).
11. R. S.-C. Su, R. J. Galas, C.-Y. Lin and J. C. Liu, Redox-Responsive Resilin-Like Hydrogels for Tissue Engineering and Drug Delivery Applications, *Macromol. Biosci.*, **19**, 1900122 (2019).
12. S. D. Mu, Q. J. Ling, X. Liu, J. Ruiz, D. Astruc and H. B. Gu, Supramolecular redox-responsive substrate carrier activity of a ferrocenyl Janus device, *J. Inorg. Biochem.*, **193**, 31 (2019).
13. R. Y. Zhang, X. Li, K. W. He, X. Y. Sheng, S. Deng, Y. Q. Shen, G. J. Chang and X. Ye, Preparation and properties of redox responsive modified hyaluronic acid hydrogels for drug release, *Polym. Adv. Technol.*, **28**, 1759 (2017).
14. Y. R. Long, B. Song, C. T. Shi, W. T. Liu and H. B. Gu, AuNPs composites of gelatin hydrogels crosslinked by ferrocene-containing polymer as recyclable supported catalysts. *J. Appl. Polym. Sci.*, **137**, 48653 (2020).
15. S. D. Mu, W. T. Liu, L. Zhao, Y. R, Long and H. B. Gu, Antimicrobial AgNPs Composites of Gelatin Hydrogels Crosslinked by Ferrocene-Containing Tetrablock Terpolymer, *Polymer*, **169**, 80 (2019).
16. D. Astruc, The supramolecular redox functions of metallomacromolecules, *J. Leather Sci. Eng.*, **2**, 13 (2020).
17. Z. Y. Yuan, J. Wang, Y. M. Wang, Y. J. Zhong, X. S. Zhang, L. Li, J. Y. Wang, S. F. Lincoln and X. H. Guo, Redox-Controlled Voltage Responsive Micelles Assembled by Noncovalently Grafted Polymers for Controlled Drug Release, *Macromolecules*, **52**, 1400 (2019).
18. T. Noyhouzer, C. L'Homme, I. Beaulieu, S. Mazurkiewicz, S. Kuss, H.-B. Kraatz, S. Canesi and J. Mauzeroll, Ferrocene-modified phospholipid: an innovative precursor for redox-triggered drug delivery vesicles selective to cancer cells, *Langmuir*, **32**, 4169 (2016).
19. R. H. Staff, M. Gallei, M. Mazurowski, M. Rehahn, R. Berger, K. Landfester and D. Crespy, Patchy Nanocapsules of Poly(vinylferrocene)-Based Block Copolymers for Redox-Responsive Release, *ACS Nano*, **6**, 9042 (2012).
20. Y. Xu, L. Wang, Y.-K. Li and C.-Q. Wang, Oxidation and pH responsive nanoparticles based on ferrocene-modified chitosan oligosaccharide for 5-fluorouracil delivery, *Carbohydr. Polym.*, **114**, 27 (2014).
21. J. Song, D. Jańczewski, Y. Y. Guo, J. W. Xu and G.J. Vancso, Redox responsive nanotubes from organometallic polymers by template assisted layer by layer fabrication, *Nanoscale*, **5**, 11692 (2013).
22. J. Song, D. Jańczewski, Y. Ma, M. Hempenius, J. Xua and G. J. Vancso, Redox-controlled release of molecular payloads from multilayered organometallic polyelectrolyte films, *J. Mater. Chem. B*, **1**, 828 (2013).
23. M. F. Ni, N. Zhang, W. Xia, X. Wu, C. H. Yao, X. Liu, X. Y. Hu, C. Lin and L. Y. Wang, Dramatically Promoted Swelling of a Hydrogel by Pillar[6]arene-Ferrocene Complexation with Multistimuli Responsiveness, *J. Am. Chem. Soc.*, **138**, 6643 (2016).
24. Y.-K. Li, C.-G. Guo, L. Wang, Y. Q. Xu, C.-Y. Liu and C.-Q. Wang, A self-healing and multi-responsive hydrogel based on biodegradable ferrocene-modified chitosan, *RSC Adv.*, **4**, 55133 (2014).
25. G. R. Qiu, X. Liu, B. R. Wang, H. B. Gu and W. X. Wang, Ferrocene-Containing Amphiphilic Polynorbornenes as Biocompatible Drug Carriers, *Polym. Chem.*, **10**, 2527 (2019).
26. X. Liu, F. F. Liu, Y. L. Wang and H. B. Gu, Ferrocene-containing amphiphilic dendronized random copolymer as efficient stabilizer for reusable gold nanoparticles in catalysis, *React. Funct. Polym.*, **143**, 104325 (2019).
27. L. C. Liu, L. L. Rui, Y. Gao and W. A. Zhang, Self-assembly and disassembly of a redox-responsive ferrocene-containing amphiphilic block copolymer for controlled release, *Polym. Chem.*, **6**, 1817 (2015).
28. Y. Kang, Y. Ma, S. Zhang, L.-S. Ding and B.-J. Li, Dual-stimuli-responsive nanoassemblies as tunable releasing carriers, *ACS Macro Lett.*, **4**, 543 (2015).
29. L. Zhang, G. R. Qiu, F. F. Liu, X. Liu, S. D. Mu, Y. R. Long, Q. X. Zhao, Y. Liu and H. B. Gu,Controlled ROMP synthesis of side-chain ferrocene and adamantane-containing diblock copolymer for the construction of redox-responsive micellar carriers, *React. Funct. Polym.*, **132**, 60 (2018).
30. X. Liu, G. R. Qiu, L. Zhang, F. F. Liu, S. D. Mu, Y. R. Long, Q. X. Zhao, Y. Liu, and H. B. Gu, Controlled ROMP Synthesis of Ferrocene-Containing Amphiphilic Dendronized Diblock Copolymers as Redox-Controlled Polymer Carriers, *Macromol. Chem. Phys.*, **219**, 1800273 (2018).
31. S. J. Zhen, X. Q. Yi, Z. J. Zhao, X. D. Lou, F. Xia and B. Z. Tang, Drug delivery micelles with efficient near-infrared photosensitizer for

combined image-guided photodynamic therapy and chemotherapy of drug-resistant cancer, *Biomaterials*, **218**, 119330 (2019).

32. K. Wang, Y. T. Hao, Y. N. Wang, J. Y. Chen, L. Z. Mao, Y. D. Deng, J. L. Chen, S. J. Yuan, T. T. Zhang, J. Y. Ren and W. Z. Liao, Functional Hydrogels and Their Application in Drug Delivery, Biosensors, and Tissue Engineering, *Int. J. Polym. Sci.*, **2019**, 3160732 (2019).
33. M. E. Wechsler, R. E. Stephenson, A. C. Murphy, H. F. Oldenkamp, A. Singh and N. A. Peppas, Engineered microscale hydrogels for drug delivery, cell therapy, and sequencing, *Biomed. Microdevices*, **21**, 31 (2019).
34. H. Hamedi, S. Moradi, S. M. Hudson and A. E. Tonelli, Chitosan based hydrogels and their applications for drug delivery in wound dressings: A review, *Carbohydr. Polym.*, **199**, 445 (2018).